

Surface Structure Patterning for Fabricating Non-fluorinated Superhydrophobic Cellulosic Membranes

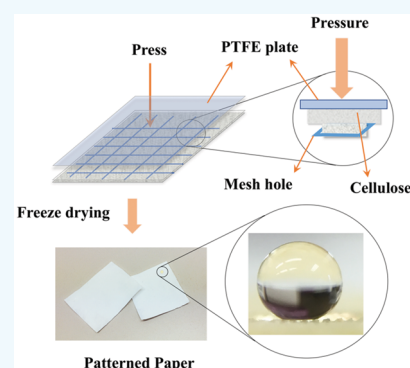
Wei Liu,¹ Feifei Sun, Lu Jiang,¹ J. Carson Meredith,¹ and Yulin Deng^{*,1}

School of Chemical & Biomolecular Engineering and RBI, Georgia Institute of Technology, 500 10th Street N.W., Atlanta, Georgia 30332, United States

S Supporting Information

ABSTRACT: Superhydrophobic surfaces have attracted great interest in both scientific research and industrial applications. Patterned nanocellulose membrane surfaces were fabricated by a simple pressing process. After chemical modification with non-fluorinated and low-cost industrial chemicals, such as alkyl ketene dimers (AKD), wax, and isocyanate, some nanocellulose membranes showed water contact angles $>150^\circ$. The combination of micro-sized pattern and nanosized cellulose fibers created a hierarchical structure that contributed to the superhydrophobic properties. SEM and optical microscopy were used to characterize the fiber network and hierarchical structures. Wetting experiments showed that water droplets roll off the cellulose membrane with fabricated pillar size lower than $100\ \mu\text{m}$ after chemical modification with AKD, wax, or isocyanate. The process used in this superhydrophobic cellulose membrane fabrication is simple, cost-effective, and amenable to scale up so it has potential to be used as a liquid packaging material.

KEYWORDS: surface patterning, template method, nanocellulosic membrane, non-fluorinated, superhydrophobicity



1. INTRODUCTION

Natural cellulose materials (e.g., cotton and wood fiber) have been used in broad applications, such as paper manufacturing, textiles, packing and building materials, and so on. Compared to the synthetic petroleum-derived fibers, cellulose materials have the advantages of biodegradability, renewability, and nontoxicity.^{1,2} Cellulose nanofibrils (CNF) and cellulose nanocrystals (CNC) are nanosized cellulose materials, and the abundant surface hydroxyl groups enable facile functionalization to create novel materials,³ such as stimuli-responsive nanomaterials,^{4,5} smart electronic devices, and wearable electronic device packaging.^{6,7} However, cellulose fibers are intrinsically hydrophilic and can absorb water or moisture, leading to erosion in humid environments. Fabricating hydrophobic or superhydrophobic surfaces is a promising way to enhance the moisture resistance of cellulose materials and minimize the water erosion issues, especially for the materials used in humid environments, such as packaging or building materials.

Superhydrophobic surfaces have attracted great scientific and industrial interest for decades. Many superhydrophobic surfaces have been created on silicon, glass, metal plate, metal mesh, and plastic substrates.^{8,9} For the silicon surface, well-patterned and micrometer-sized cylindrical pillar arrays and mushroom-like arrays were fabricated.^{10–12} The water contact angle can reach very high because of the re-entrant structure in the side wall of pillars. Nanoparticles and needle-like or lotus leaf-like nanostructure were introduced on a metal surface to generate the hierarchical roughness for improving the hydrophobicity.^{13–17} These results provide different rational

strategies for water-repellent or superhydrophobic fabrication. The key factors between them are surface roughness and low surface energy that can repel and support water droplet to avoid spreading.¹²

For cellulose-based material, there are various strategies that can reach superhydrophobicity. The first strategy is to increase surface roughness using nanoparticles, such as nano-SiO₂ or TiO₂ particles, through in situ wet deposition, dip coating, or spray coating on the material surface,^{18–20} but the nanoparticle aggregation and coating stability are obvious issues. Another method is to create nanoscaled roughness on the surface of fibers directly by etching, for example, plasma pretreatment.^{21–24} However, plasma treatment is a tedious and costly process that can only applied on a small scale. To achieve low surface energy, fluorine-containing compounds are commonly used in cellulose fiber modification.^{25–27} Because fluorine-containing compounds are not safe and high cost, developing an economical and facile method that does not use fluorine chemicals and easy to scale up is of great interest.

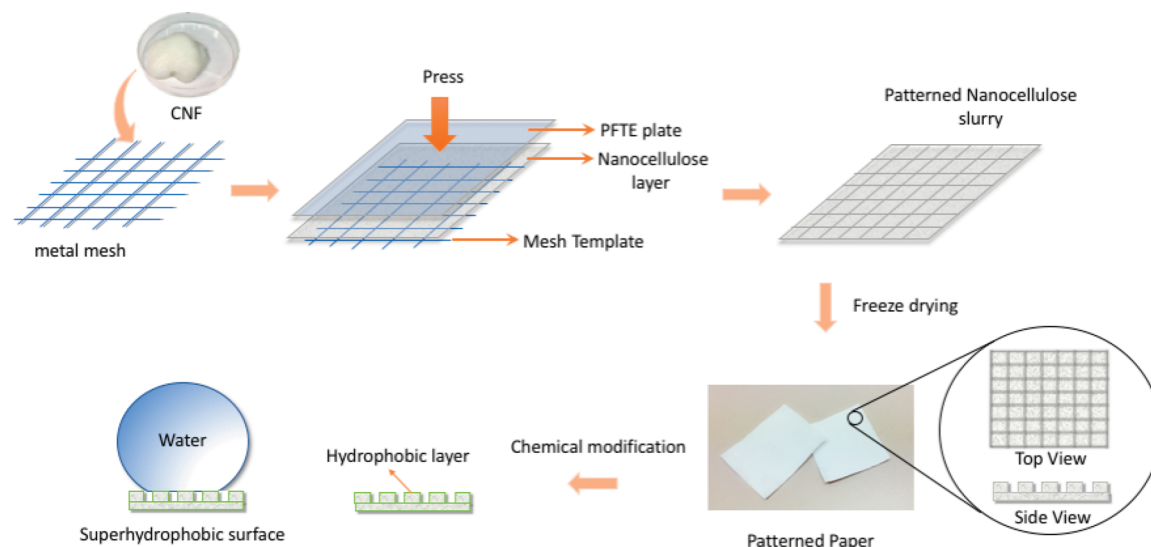
Herein, we present a facile fabrication of patterned superhydrophobic cellulose membrane with a quick templated pressing method and non-fluorinated chemical modification. The stainless-steel mesh, which possesses regularly arranged mesh holes, functions as template or mold in the pressing method. By pressing the nanocellulose slurry on the mesh, the cellulose slurry fills into the mesh holes and the shape is

Received: March 7, 2019

Accepted: April 24, 2019

Published: April 24, 2019

Scheme 1. Schematic Diagram of Pressing Process for Preparation of Patterned Surface Nanocellulose Membrane



maintained after removal from the mesh mold. After drying, the pillar featured pattern can be well-established on the surface of cellulose membrane (shown in Scheme 1). Different from the pillar array fabricated on the silicon wafer surface, cellulose fibers inherently have submicrometer or nanometer structures. The microsized pattern and nanosized cellulose fibers network create a hierarchical structure that can improve the superhydrophobic properties. After simple chemical modification with non-fluorine chemicals, such as AKD, wax, or isocyanate, the fabricated cellulose membranes show a good superhydrophobic property. This method has significant advantages: (1) The pattern fabrication by templated pressing can be quickly completed even in several seconds and is easily to scale up. (2) The featured sizes of patterns are tunable by using different mesh size of metal or plastic meshes, which is readily accessible in the industry. (3) Low-cost and non-fluorine compounds are used in chemical modification through simple heating.

2. MATERIALS AND METHODS

2.1. Materials. Cellulose nanofibril slurry (CNFs, fiber content 3.4%) prepared from mechanically refined bleached softwood Kraft pulp was purchased from the University of Maine Process Development Center. Toluene diisocyanate (TDI) was purchased from TCI America. Hexadecanol ($C_{16}OH$) and solvents toluene, benzene, and tetrahydrofuran (THF) were purchased from Alfa Aesar. Polymers, including poly(methyl methacrylate) (PMMA, $M_w \sim 200000$), polystyrene (PS, $M_w \sim 250000$), low-density polyethylene (LDPE), polypropylene (PP, $M_w \sim 230000$), and poly(vinyl chloride) (PVC, $M_w \sim 250000$), solid wax, and solid alkyl ketene dimers (AKD) are industrial grade products.

2.2. Preparation of Surface Textured Nanocellulose Membrane and Chemical Modification. Cellulose nanofibril slurry was coated on a stainless steel mesh to form a thin layer of cellulose nanofibrils with a thickness about 2–3 mm. The cellulose layer along with the mesh was pressed with a hydraulic machine under the pressure of 1 MPa and maintained for 10 s. About 70% of water in the nanocellulose slurry was removed after pressing. A half-dried cellulose membrane with pressed pattern was obtained and was frozen in liquid nitrogen for 15 min. The cellulose membrane was freeze-dried under a vacuum of 20 mTorr (VirTis Freezemobile 25EL sentry 2.0) for 1 day.

Before chemical modification, the modifier was dissolved in organic solvent to form a homogeneous solution. Eight different modifiers

were chosen for the chemical modification: PMMA, PS, PE, wax, and AKD were dissolved in toluene; PVC was dissolved in THF; PP was dissolved in benzene; and TDI and hexadecanol ($C_{16}OH$) at the molar ratio 4:1 were used as comodifiers and dissolved in toluene. All the modifier concentrations dissolved in solvents are 5 wt %. The prepared cellulose membrane was immersed in the modifier solution and heated to boiling for 5 min. After immersion, the cellulose membrane was removed from the modifier solution. Excess fluid on the membrane was then absorbed with tissue paper (KimWipe, Kimberly-Clark Co.). The obtained membrane was then placed in an oven at 100 °C for 10 min to evaporate solvent and strengthen the polymer coating layer.

To make useful comparisons, different textured paper substrates (copy paper (Staples, 92 bright), paper towel (Uline EZ Pull Sr.), and filter paper (Whatman, qualitative grade 1)) were used in the chemical modifications with AKD, wax, and TDI + $C_{16}OH$. The procedures were the same as the treatment of prepared membranes.

2.3. Template Modification for Tuning of Asperity Size and Patterned Coating on Substrate. To obtain metal meshes with different pore sizes that are not able to be purchased from the supplier, an electrodeposition of Cu on the metal meshes was conducted. Experimentally, the metal mesh was used as the working electrode which connects to the negative electrode of external direct current power source. A copper plate was used as the counter electrode connected to the positive electrode of power source. The metal mesh and copper plate were immersed in 0.1 mol L⁻¹ $CuSO_4$ solution. The deposition current was controlled at 20 mA. During the electrolysis, the copper was deposited on the metal wire of mesh. Therefore, the diameter of metal wire was increased, and the mesh hole was decreased. The electrodeposition treated metal mesh was directly used as template for tuning of asperity size in the patterned cellulose membrane fabrication.

The pattern coating was conducted on the substrate of copy paper (Staples, 92 bright). A thin layer of nanocellulose slurry (3.4 wt %) with a thickness about 2–3 mm using a doctor blade with controlled thickness was coated on copy paper substrate by a glass rode doctor blade and then covered with a mesh template. The following pressing and freeze-drying procedures were the same as the patterned cellulose membrane fabrication described in section 2.2. The pattern coated on copy paper was obtained after freeze-drying and was chemically treated with wax, AKD, or TDI + $C_{16}OH$.

2.4. Wetting Ability Measurement. The static water contact angle measurement of patterned nanocellulose membrane was performed using a contact angle goniometer (100-25-A model, ramé-hart instrument co.) at ambient environment. A droplet of 8 μ L of deionized water was placed on the prepared membrane surface for

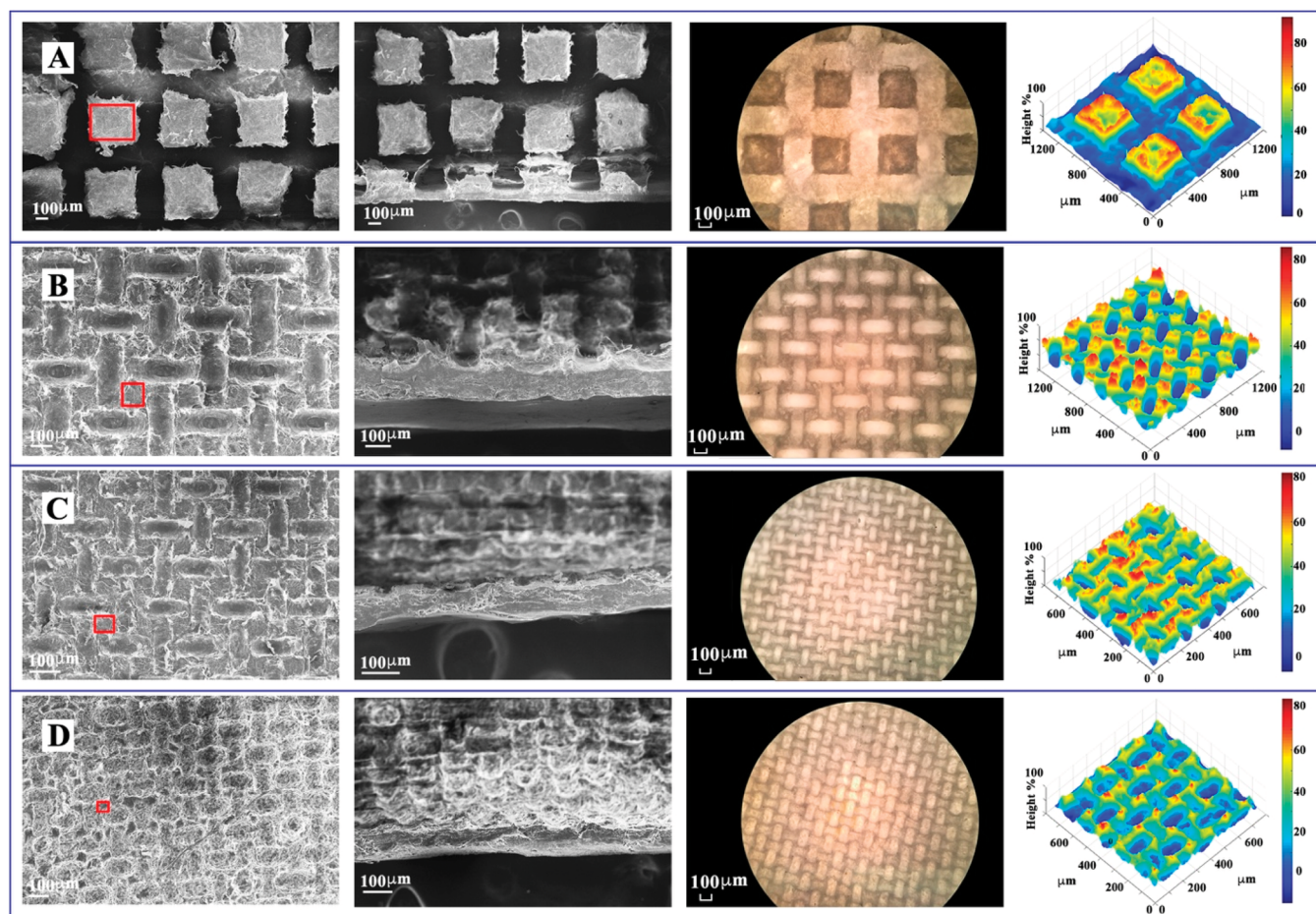


Figure 1. Top view and side view of SEM images, optical microscopy images, and 3D profile simulation (from the left to the right column) of the four different pattern sizes featured nanocellulose membranes (noted as membranes-1 to -4 in A to D, respectively).

the measurement. Dynamic advancing and receding contact angles were measured by increasing and decreasing the droplet volume, with an initial volume of $8 \mu\text{L}$ and a step change of $0.3 \mu\text{L}$. The contact angle measurements were repeated five times for each fluid. Different fluids including coffee, sweet tea, Sprite, red wine, Fanta, and Coke, which were obtained from Walmart supermarket, were used in the static contact angle measurement with $8 \mu\text{L}$ of applied fluid.

The long-time contact angle measurement and knife scratching test were completed. In the long-time contact angle measurement, $8 \mu\text{L}$ of deionized water was used, and the contact angle was continuously measured for 20 min. The scratch test was performed using a knife to longitudinally and transversely scratch the patterned surface, and then the water contact angle was measured.

2.5. Other Characterization. The surface morphology of aerogels was examined via a LEO 1530 thermally assisted field emission scanning electron microscope (FE-SEM) with an acceleration voltage of 10 kV. Samples were gold-sputtered prior to SEM images.

Optical microscopic images were obtained using a Leica DMLM light microscope connected to a color video camera. The 3D structure simulation is calculated from the brightness value of each image pixel using a Matlab program based on the condition that light linearly decays with the passed thickness cellulose membrane.

Fourier transform infrared (FTIR) spectra of both original and sulfonated aerogel samples were measured by KBr pellets on a Bruker Vertex 80V spectrometer in the scan range of $4000\text{--}400 \text{ cm}^{-1}$ of 32 scans with resolution 4 cm^{-1} .

Thermogravimetric analysis (TGA) and derivative thermogravimetric (DTG) analysis were performed using a PerkinElmer STA600 simultaneous thermal analyzer to evaluate thermal degradation of

original and sulfonated sample in the range $40\text{--}600 \text{ }^\circ\text{C}$ at a rate of $10 \text{ }^\circ\text{C}/\text{min}$ under a nitrogen flow rate of 20 mL min^{-1} .

3. RESULTS AND DISCUSSION

3.1. Morphology of Surface Roughness. Figure 1 shows the patterned surface of the cellulose membranes with four different characteristic pattern sizes (noted as membranes-1 to -4 in A to D, respectively). The left column and the second left column show the top view and side view of SEM images. From the top view images, the cellulose membrane surfaces exhibit a lattice-like pattern that is molded by the stainless mesh. The islands highlighted by red lines are molded pillar locations. The 3D structures are clearly illustrated from the side view, which shows regularly arranged square pillars distributed on the surface of nanocellulose membrane. Four different meshes with various mesh sizes were used for the pillar patterns fabrication. For the membranes from 1 to 4, the pillars show different widths of 349.5 ± 3.5 , 110.0 ± 4.7 , 60.1 ± 2.9 , and $36.3 \pm 3.7 \mu\text{m}$, respectively (summarized in Table S1). The pillar heights of the four different membranes are 70.7 ± 3.2 , 39.3 ± 4.1 , 19.5 ± 3.1 , and $19.8 \pm 2.9 \mu\text{m}$ according to the side view of SEM images.

The optical microscopy images of the four different membranes are shown in the third left column in Figure 1. The images illustrate bright and dark patterns based on the light transmission. The thicker the location is, the darker it will appear in the image because of the light absorbance and light

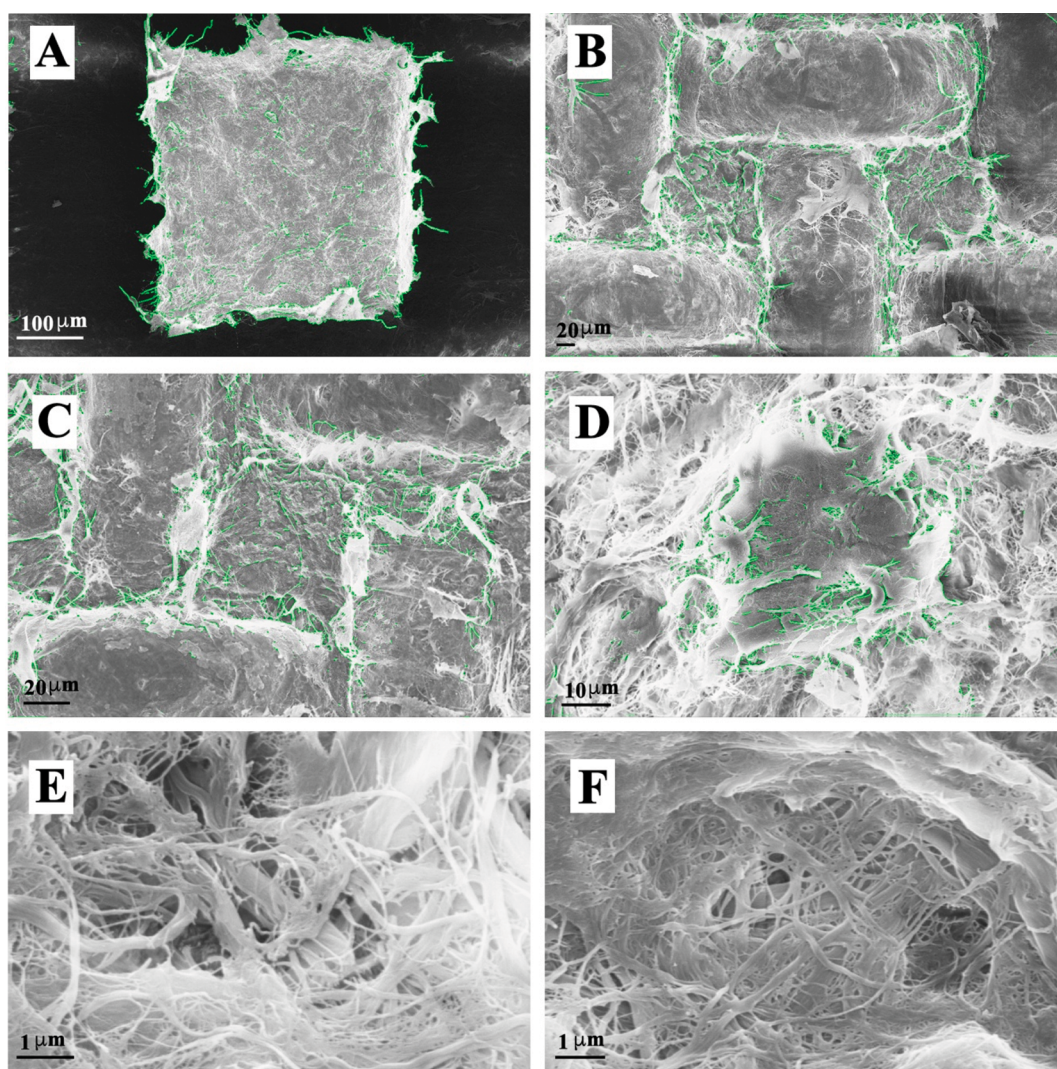


Figure 2. Magnified SEM images of the Nano cellulose pillars. (A–D) Pillar on the nanocellulose membranes-1 to -4 respectively. (E, F) Typical SEM images of nanocellulose fibers (came from membranes-2 and -3). The nanocellulose fiber edge was highlighted with green color which was generated by a Matlab program.

scattering. We obtained four different optical microscopy patterns that are similar to the SEM top view images. According to Beer–Lambert’s law, the transmittance, which reflects brightness in the image, depends on the light transmitted path length through the membrane. Assuming that the light transmittance has a linear relationship with the light path length, the thickness profile of the membranes can be calculated based on the brightness data of optical microscopy images. The simulation results are shown in the right column in Figure 1. The red color shows high thickness locations, and the blue color shows the places with low thickness. The simulation results reveal the 3D profiles of pillar-like patterns on the nanocellulose membranes.

Different from the pillar array built on the Si wafer,^{10,28} the mesh molded nanocellulose pillars do not have a smooth surface because nanocellulose fibers are inherently in Nanosize. As a result, nano- and submicrometer scaled roughness are presented on the molded pillars surface. Figure 2 shows the magnified SEM images of the cellulose pillars. We can see that the pillar surface is not perfectly smooth but plenty of nanocellulose fibers randomly distributed on it. The magnified 3D surface profile simulation clearly shows the submicrometer

roughness on top of the patterned pillar (shown in Figure S1). The nanocellulose fibers were shown in magnified SEM images E and F in Figure 2. The diameter is several nanometers. Because of the surface –OH groups of cellulose nanofibers, agglomerated bundles are formed by H-bondings between neighboring nanofibers. Therefore, the cellulose pillar maintains molded shape after removing the mesh template. Cellulose pillars constitute the ordered pillar array and disordered nanofibers contribute to the nanoscaled roughness on each pillar. Herein, multiple scaled roughness and patterned structure are fabricated on the cellulose membrane.

3.2. Wettability of Patterned Cellulose Membrane after Chemical Modification. To obtain superhydrophobic performance, chemical modification was conducted on the patterned membrane surface since modification changes the surface energy. Different polymers and chemicals, including PMMA, PS, PP, PE, PVC, wax, AKD, and isocyanate agent, were applied. To compare with the patterned surface, the polymers and chemicals were coated on glass slides to make smooth coated surfaces. The static water contact angles were measured on different coated smooth surfaces and patterned membrane-2, respectively, as shown in Figure 3A. It can be

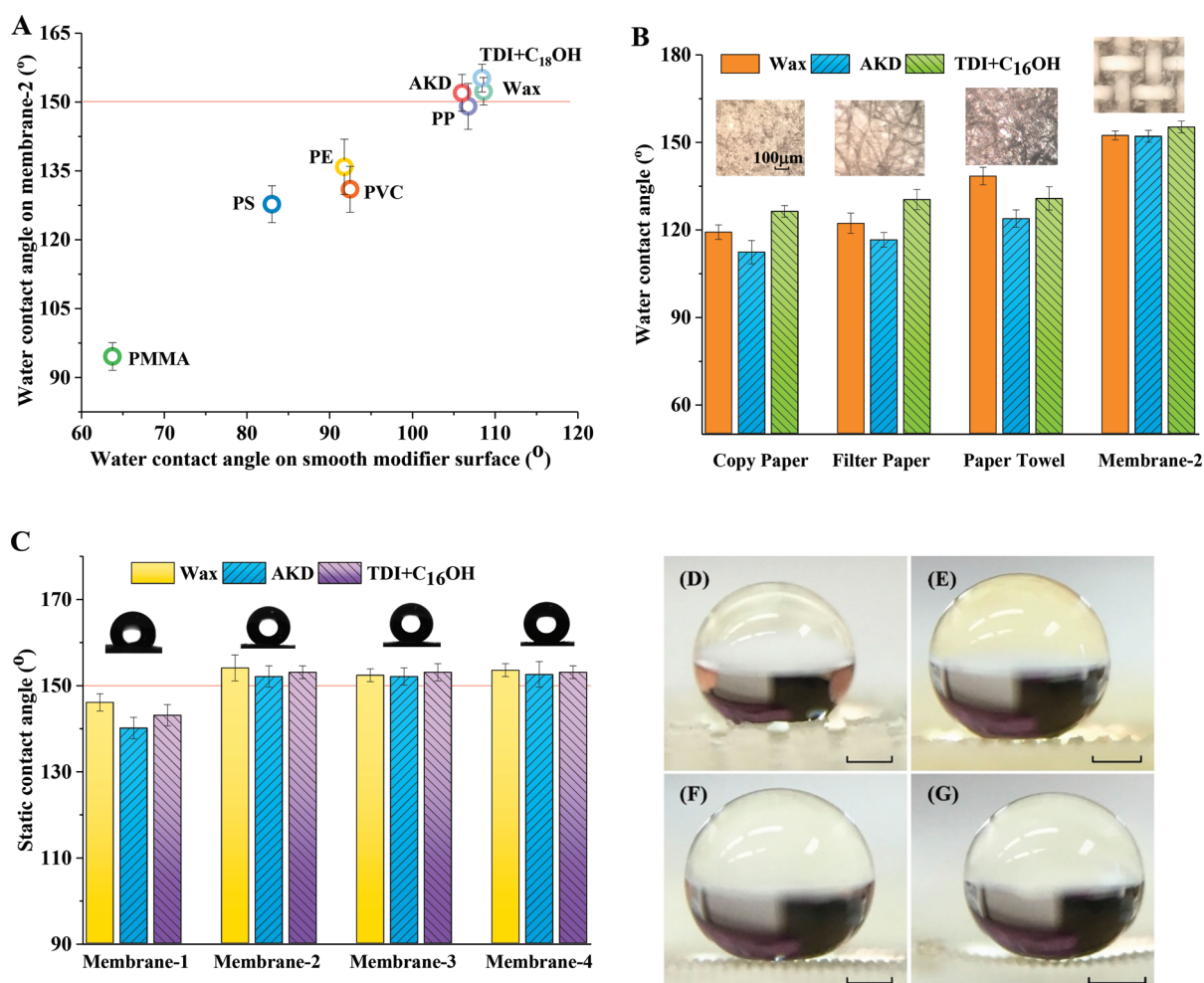


Figure 3. (A) Plot of static water contact angles on modified smooth surface and patterned cellulose membrane. (B) Water contact angle comparisons of patterned membrane with different papers. Insets: microscopy images of copy paper, filter paper, paper towel, and patterned membrane-2. (C) Water contact angles of four different patterned nanocellulose membranes. Insets: photographs of the water droplets sitting on wax modified membranes. (D–G) Magnified photograph of the solid–water–air interface of patterned membranes-1 to -4, respectively (scale bar 400 μm).

concluded that, first, the patterned roughness can increase the hydrophobicity. For example, the water contact angle on the PS-coated smooth surface is 83° , but on the prepared patterned membrane the water contact angle increases to 130° . Second, the more hydrophobic the applied chemicals are, the higher the contact angle can be obtained. After modifications with AKD, wax, or isocyanate, the resulting contact angles of patterned membrane-2 are higher than 150° , indicating the superhydrophobic property.

Compared with copy paper, filter paper, and paper towel, the patterned nanocellulose membrane shows an outstanding hydrophobic performance since the contact angles for the three kinds of representative papers are only around 120° – 130° even after AKD, wax, or isocyanate modifications, as shown in Figure 3B. The microscopy images of the chosen papers were inserted to Figure 3B. As can be seen, the copy paper has a relatively smooth surface and plenty of particle fillers attached the fibers. The images show that filter paper is composed of long fibers and paper towel has some broken fibers. The superhydrophobic behavior of prepared membrane-2 is ascribed to the patterned roughness which is shown in the inserted image in Figure 3B. Without the patterned roughness, the CNF membranes which have the same drying and chemical

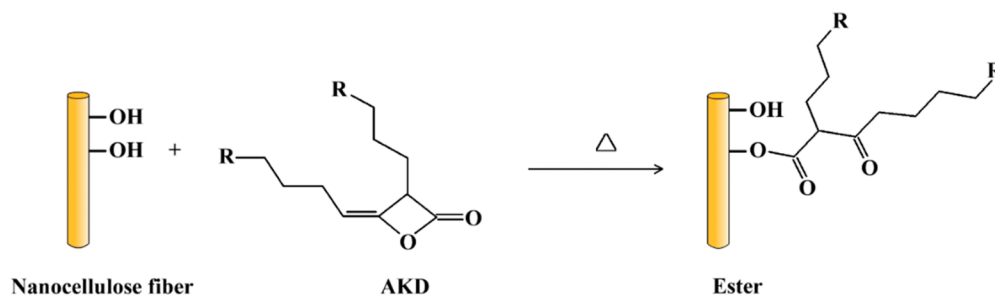
treatment processes cannot reach superhydrophobicity, showing the water contact angle 99° – 113° (Figure S2).

The water wettability of four different nanocellulose membranes templated by four different sized meshes was measured. As exhibited in Figure 3C, after modifications with three different chemicals, including AKD, wax, and isocyanate, the prepared membranes have a high water contact angle except for membrane-1. This is because the membrane-1 has a big pillar size that cannot support the water repellent to superhydrophobic. Decreasing the pillar size, as the membranes-2 to -4 show, the water contact angles increased to $>150^{\circ}$. The obtained membrane-2 can reach a 150° water contact angle and has a large surface pattern size ($\sim 110 \mu\text{m}$) that is easy to fabricate; therefore, membrane-2 was chosen as a representative membrane used in the following studies.

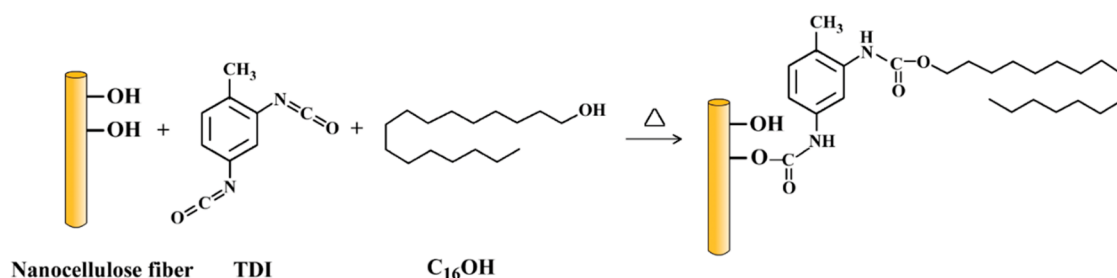
Figure 3D–G shows magnified solid–air–water interfaces when the water droplets sat on the surfaces of four different prepared membranes. It can be clearly seen that the water droplet on the top of the asperities and the air packages are trapped below the droplet, suggesting the Cassie–Baxter state on the membrane surface.

3.3. FT-IR and TGA Characterizations. With AKD modification, the long alkane chain of AKD can react with

• AKD (Alkyl ketene dimer) modification



• Isocyanate reagent



• Wax and polymer coating
Absorption, no reaction.

Figure 4. Chemical reactions between cellulose fiber and the modifiers (AKD and TDI + C₁₆OH).

the hydroxyl group of nanocellulose fibers through ester bonding and then graft on the fiber surfaces, as shown in Figure 4 and discussed later. In TDI + C₁₆OH modification, the TDI molecule acts as a bridge that connects with the C₁₆OH and nanocellulose fibers. However, wax modification is a physical absorption process without chemical reaction.

The chemical structure changes of modified membranes can be verified by FT-IR spectroscopy (Figure 5A). The spectrum of native cellulose membrane shows the O–H stretching vibration at 3440 cm⁻¹ and the C–O stretching vibration at 1060 cm⁻¹. Moreover, the spectrum shows a characteristic peak of β -glycosidic bond absorption at 895 cm⁻¹ and cellulose characteristic peaks at 2920 and 1634 cm⁻¹.²⁹

Different absorption peaks were observed from the FT-IR spectra of modified nanocellulose membranes. For the spectrum of wax modified membrane, the bands at 2921, 2848, 1469, and 724 cm⁻¹ show the presence of C–H stretching vibration of CH₂ in a long-chain alkyl group. The AKD modified membrane showed the same C–H stretching peaks as wax because of the long-chain alkyl groups in AKD molecule that gives the AKD good hydrophobicity. In addition, the characteristic peak at 1722 cm⁻¹ can be ascribed to the absorption of β -ketone ester, indicating that AKD has reacted with hydroxyl groups on the surface of cellulose.^{30,31} In the modification by isocyanate, the formed product should be carbamates with the hydroxyl groups of hexadecanol and cellulose. Therefore, in the spectra of TDI + C₁₆OH membrane, the occurrence of peaks at 1691 cm⁻¹ can be ascribed to the stretching vibration of C=O in carbamates, but the absorption of the aromatic ring and the groups attached to the amide nitrogen atoms are not easy to detect in this case.

Thermogravimetric (TG) curves of chemically modified membranes are shown in Figure 5B. As can be seen from the TG curve of initial nanocellulose membrane, the weight loss was nearly 100% after the temperature reaches 700 °C. The derivative thermogravimetric curve indicated that the temperature at the maximum decomposition rate for initial nanocellulose membrane was 350 °C. For chemical modified membranes, the temperature value at the maximum decomposition rate was slightly increased, as shown in Figure 5C. In addition, the loss of a small amount of volatile components can be seen in the decomposition temperature of 200–300 °C for chemical modified membranes.

3.4. Tuning of Asperity Size and Patterned Coating on Substrate. Metal meshes with different mesh sizes were used as templates to fabricate the patterned membranes-1 to -4. The templates can be modified as well by copper electrodeposition, for the purpose of membrane asperity size tuning. The diameter of mesh wires was increased after the electrodeposition, and the hole opening of metal mesh was decreased. By this way, the asperity size, i.e., the width of patterned pillar and the gap between neighboring pillars, can be controlled. The obtained mesh templates after copper electrodeposition and prepared nanocellulose membranes-5 and -6 by using modified templates are shown in the Supporting Information (Figures S3 and S4). The gap between two molded pillars was increased from 127 μ m of membrane-2 to 150 μ m of membrane-5 and further to 191 μ m of membrane-6 (summarized in Table S1). In addition, the corresponding pillar width was decreased from 108 to 89 μ m and further to 49.5 μ m, leading to a decrease of solid area fraction on surface. The solid area fraction refers to the geometric top area of pillars to the total geometric area of membrane, which is a key parameter to affect the hydro-

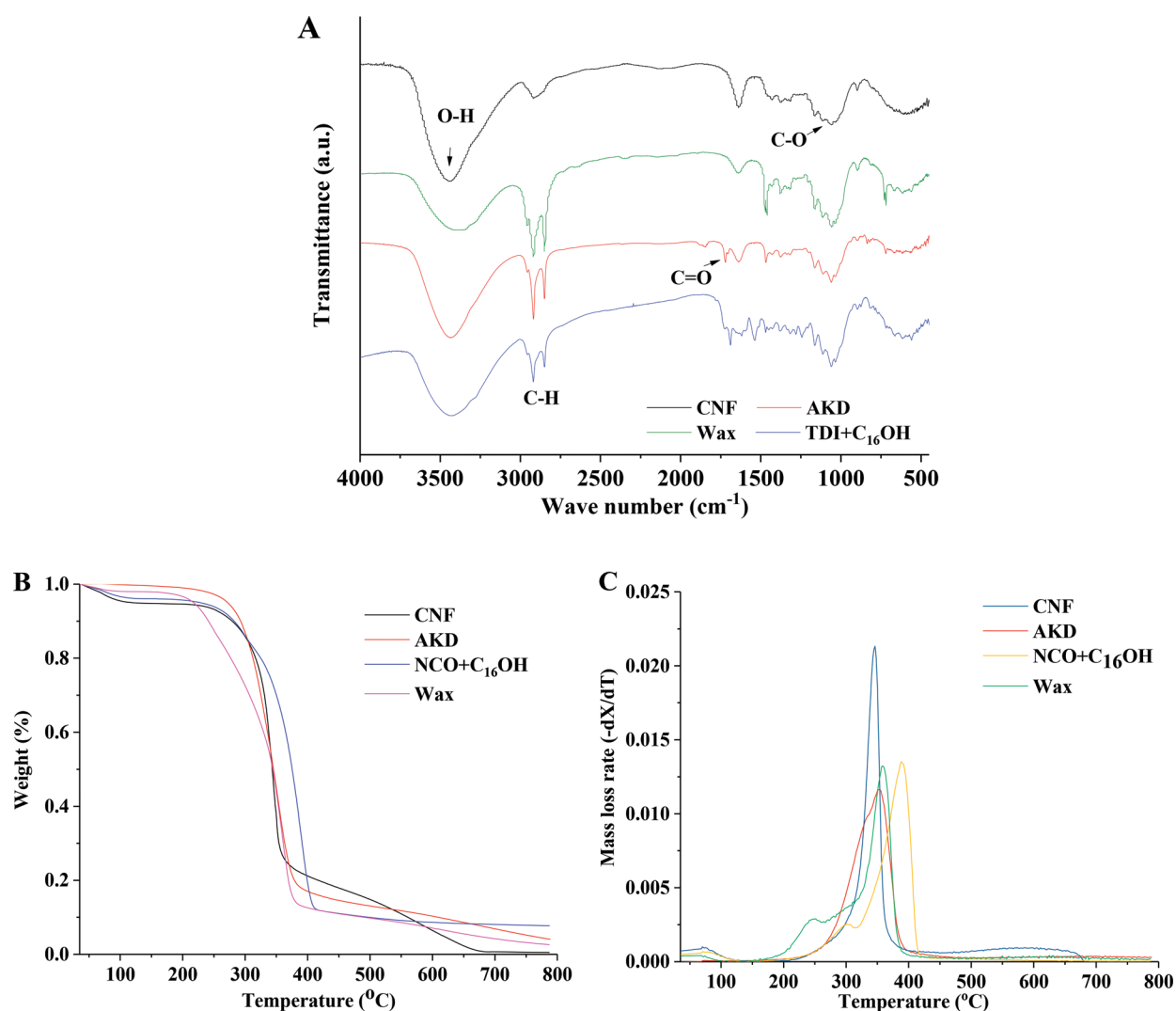


Figure 5. (A) Fourier transform infrared (FT-IR) spectra, (B) thermogravimetric curves, and (C) derivative thermogravimetric curves of initial and chemical modified membrane-2.

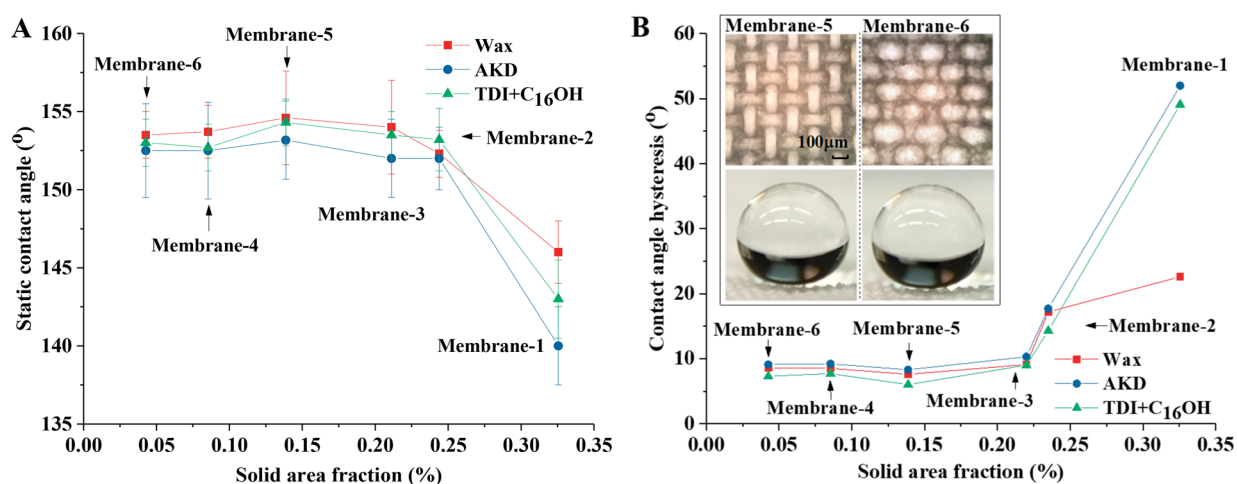


Figure 6. (A) Static contact angles of chemical modified membranes-1 to -6 with different surface solid area fractions. (B) Contact angle hysteresis of prepared membranes-1 to -6. Insets: optical microscopic images of membranes-5 and -6 (top) and the interface images of water droplets sitting on the surface (bottom).

phobicity. The measured static contact angles of membrane-1 to -6 versus surface solid area fraction are plotted in Figure 6A.

The surface solid area fraction decreases from 0.33 to 0.04 in the order of membranes-1, -2, -3, -5, -4, and -6. With the

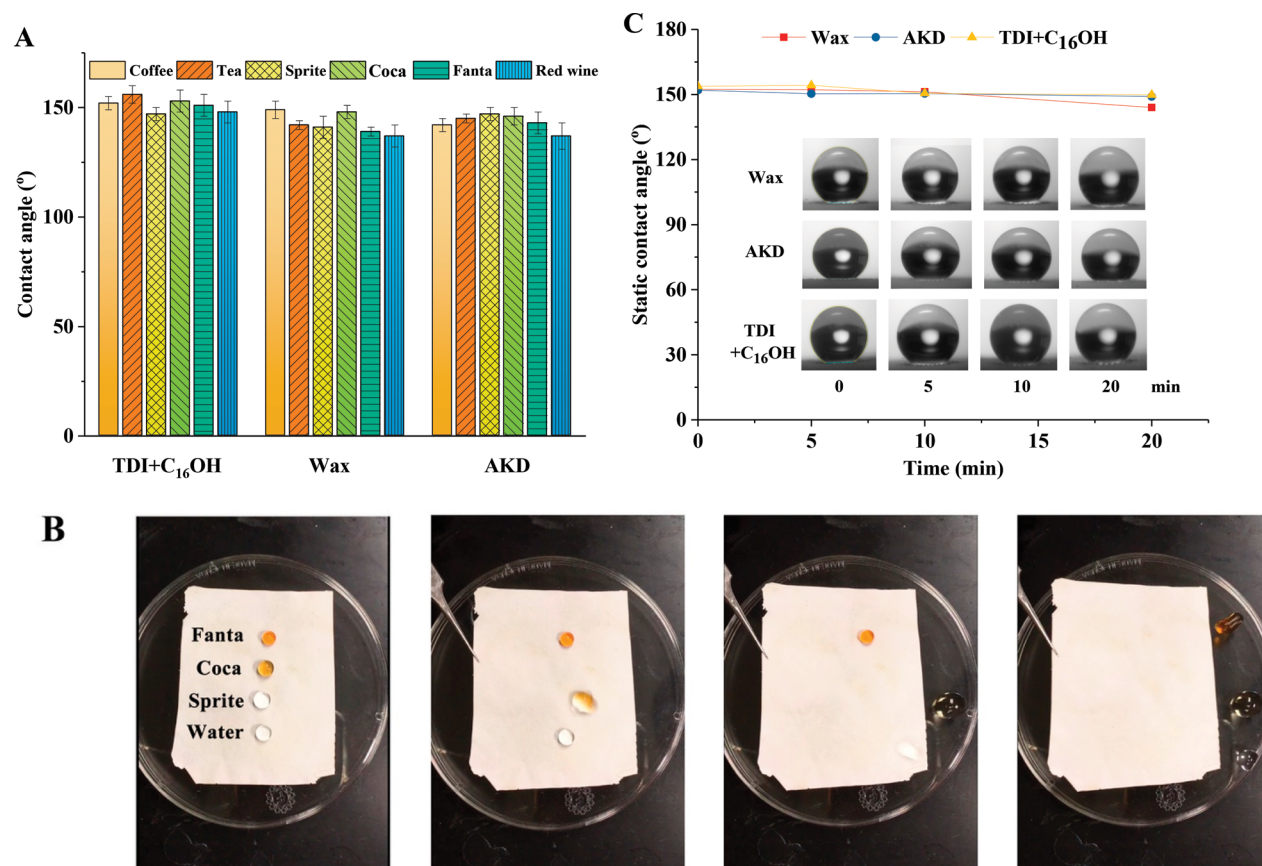


Figure 7. (A) Static contact angles of different solutions on chemical modified membrane-2. (B) Dynamic process of different liquids rolling off isocyanate modified membrane-2. (C) Plots of water contact angle versus contact time on the modified membrane-2. Insets: photographs of the water drops sat on the membrane-2.

decrease of solid area fraction, the static water contact angle increases. The membranes with wax modification have slightly higher contact angles than that of membranes with the modification of TDI + C₁₆OH and AKD at the same characteristic sizes of pillars. But the contact angles with three different chemical modifications are all >150°, which means superhydrophobicity when the solid area fraction is lower than 0.25. The contact angle hysteresis (CAH), defined as the difference between the advancing and receding contact angle in a dynamic process, is an important parameter to characterize superhydrophobic surfaces. Low CAH indicates the low friction for water droplet rolls off the surface. The CAH in this study is summarized in Figure 6B, showing that the CAH drops with the decrease of solid area fraction. Although the membrane-2 has a high static contact angle over 150°, the CHA value is still high (>10°). When the solid area fraction is lower than 0.21 (membranes-3, -4, -5, and -6), the CHA value drops to lower than 10°, which means a very low moving fraction for water droplets and possibly forms a self-clean surface. The optical microscopic images of membranes-5 and -6 and the interface images of water droplets sat on the surface are inserted in Figure 6B.

The patterned surface can also be coated on substrates to form a composite membrane. By simply putting nanocellulose slurry on the surface of substrates and then templated pressing, the pattern layer can be formed on the substrate surface. In this study, a patterned composite membrane was fabricated by combining a microfiber copy paper layer and a patterned nanocellulose layer (as shown in Figure S5). After modification

with wax, the measured static water contact angle reached over 150°, verifying a superhydrophobicity which is the same as prepared nanocellulose membranes.

3.5. Wettability for Other Solutions and Stability.

Besides water, several liquids that are common sources of stains in daily life were applied to investigate the wettability of the prepared membrane. Figure 7A includes the contact angles of solutions of coffee, tea, Sprite, Coca-Cola, Fanta, and red wine. It is important to note that the surface tension of these solutions are varied because some salts and organics are dissolved in the solutions, such as sugar in Sprite, Coca-Cola, and Fanta, alcohol in red wine, and caffeine in coffee and tea. The surface tension of the solutions may be decreased or increased compared with that of water. Therefore, the measured contact angles fluctuate around 140°–150°, as shown in Figure 7A. In general, most of the chosen solutions have high contact angles on prepared membrane-2. More importantly, the solution drops can easily roll off the prepared membranes without significant adhesion. Figure 7B and Figure S6 show dynamic rolling-off processes of different solutions from isocyanate reagent modified membrane-2, suggesting that prepared membrane cannot be contaminated by these soft drinks so it should be used as soft drink containers.

The contact time effect was also investigated on the chemical modified membrane-2. As we can see from Figure 7C, the water contact angles for AKD and isocyanate modified membrane-2 maintain stable as the water contact time increases from 0 to 20 min. The wax modified membrane shows a little decrease, but the contact angles are still around

150° after 20 min contact time. The physical coating of wax modification but not chemical bonding can explain the slight decrease of water contact angle. Different from wax, the AKD and isocyanate reagent can chemically bond with the surface –OH group of cellulose to form a chemically stable structure that can maintain high water contact angles during long contact time. The knife scratching test was also performed according to the literature methods.^{19,32,33} After scratching by a knife, the membrane surface was cut and broken (see Figure S7), but the patterned pillars were not completely removed. The measured water contact angle was slightly decreased to 145°–149°, and the water droplets can smoothly droll off the tilted surface in the testing (Figure S7).

4. CONCLUSION

In summary, patterned nanocellulose membranes were fabricated by a fast template pressing method. The superhydrophobicity of prepared membranes was supported by (1) the micro-sized pattern and nano-sized fibers formed hierarchical roughness structures and (2) the low surface energy after chemical modification with long alkane chains. The prepared membrane showed a good repellent ability to water and common stain fluids and good hydrophobic behavior in the long-time measurement and knife scratch testing. The asperity size of patterns was tuned by modification of the templates by electrodeposition, and the patterned surface was extended to be used as a coating layer on substrates. By this way, the patterned surface can be potentially employed in the packaging industry due to the economic, fast, and environmentally friendly process.

■ ASSOCIATED CONTENT

Supporting Information

The Supporting Information is available free of charge on the ACS Publications website at DOI: 10.1021/acsapm.9b00215.

3D profile simulations, illustration of copper electro-deposition device, SEM images and 3D profile simulations of size-tuned membrane, SEM images of patterned layer coated on copy paper substrate, scratched membranes and parameters of patterned membranes (PDF)

■ AUTHOR INFORMATION

Corresponding Author

*E-mail yulin.deng@rbi.gatech.edu.

ORCID

Wei Liu: 0000-0002-8209-5191

Lu Jiang: 0000-0002-4106-8293

J. Carson Meredith: 0000-0003-2519-5003

Yulin Deng: 0000-0002-1797-7702

Author Contributions

Y.L.D. and W.L. conceived the project and designed the experiments. W.L. and F.F.S. prepared the patterned nanocellulose membranes and tested the wetting ability of membranes. J.L. performed dynamic contact angle measurements. W.L., J.C.M., and Y.L.D. contributed to the manuscript.

Notes

The authors declare no competing financial interest.

■ REFERENCES

- (1) Kim, J.-H.; Shim, B. S.; Kim, H. S.; Lee, Y.-J.; Min, S.-K.; Jang, D.; Abas, Z.; Kim, J. Review of nanocellulose for sustainable future materials. *International Journal of Precision Engineering and Manufacturing-Green Technology* **2015**, *2* (2), 197–213.
- (2) Abdul Khalil, H. P. S.; Bhat, A. H.; Ireana Yusra, A. F. Green composites from sustainable cellulose nanofibrils: A review. *Carbohydr. Polym.* **2012**, *87* (2), 963–979.
- (3) Weibing, W.; Lei, Z. Functionalization and Applications of Nanocrystalline Cellulose. *Prog. Chem.* **2014**, *26* (0203), 403–414.
- (4) Ye, C.; Malak, S. T.; Hu, K.; Wu, W.; Tsukruk, V. V. Cellulose Nanocrystal Microcapsules as Tunable Cages for Nano- and Microparticles. *ACS Nano* **2015**, *9* (11), 10887–10895.
- (5) Wu, W.; Huang, F.; Pan, S.; Mu, W.; Meng, X.; Yang, H.; Xu, Z.; Ragauskas, A. J.; Deng, Y. Thermo-responsive and fluorescent cellulose nanocrystals grafted with polymer brushes. *J. Mater. Chem. A* **2015**, *3* (5), 1995–2005.
- (6) Qiu, X.; Hu, S. “Smart” Materials Based on Cellulose: A Review of the Preparations, Properties, and Applications *Materials* **2013**, *6* (3), 738.
- (7) Kim, J.; Yun, S.; Ounaies, Z. Discovery of Cellulose as a Smart Material. *Macromolecules* **2006**, *39* (12), 4202–4206.
- (8) Li, S.; Huang, J.; Chen, Z.; Chen, G.; Lai, Y. A review on special wettability textiles: theoretical models, fabrication technologies and multifunctional applications. *J. Mater. Chem. A* **2017**, *5* (1), 31–55.
- (9) Yu, S.; Guo, Z.; Liu, W. Biomimetic transparent and superhydrophobic coatings: from nature and beyond nature. *Chem. Commun.* **2015**, *51* (10), 1775–94.
- (10) Tuteja, A.; Choi, W.; Mabry, J. M.; McKinley, G. H.; Cohen, R. E. Robust omniphobic surfaces. *Proc. Natl. Acad. Sci. U. S. A.* **2008**, *105* (47), 18200–18205.
- (11) Liu, T. L.; Kim, C.-J. C. Turning a surface superrepellent even to completely wetting liquids. *Science* **2014**, *346* (6213), 1096–1100.
- (12) Tuteja, A.; Choi, W.; Ma, M.; Mabry, J. M.; Mazzella, S. A.; Rutledge, G. C.; McKinley, G. H.; Cohen, R. E. Designing Superoleophobic Surfaces. *Science* **2007**, *318* (5856), 1618–1622.
- (13) Zhang, L.; Zhong, Y.; Cha, D.; Wang, P. A self-cleaning underwater superoleophobic mesh for oil-water separation. *Sci. Rep.* **2013**, *3*, 2326.
- (14) Tian, D.; Zhang, X.; Tian, Y.; Wu, Y.; Wang, X.; Zhai, J.; Jiang, L. Photo-induced water-oil separation based on switchable superhydrophobicity-superhydrophilicity and underwater superoleophobicity of the aligned ZnO nanorod array-coated mesh films. *J. Mater. Chem.* **2012**, *22* (37), 19652.
- (15) Jiang, L.; Zhao, Y.; Zhai, J. A Lotus-Leaf-like Superhydrophobic Surface: A Porous Microsphere/Nanofiber Composite Film Prepared by Electrohydrodynamics. *Angew. Chem.* **2004**, *116* (33), 4438–4441.
- (16) Choi, H.-J.; Shin, J.-H.; Choo, S.; Ryu, S.-W.; Kim, Y.-D.; Lee, H. Fabrication of superhydrophobic and oleophobic Al surfaces by chemical etching and surface fluorination. *Thin Solid Films* **2015**, *585*, 76–80.
- (17) Li, L.; Li, B.; Dong, J.; Zhang, J. Roles of silanes and silicones in forming superhydrophobic and superoleophobic materials. *J. Mater. Chem. A* **2016**, *4* (36), 13677–13725.
- (18) Hou, Y.; Wang, Z.; Guo, J.; Shen, H.; Zhang, H.; Zhao, N.; Zhao, Y.; Chen, L.; Liang, S.; Jin, Y.; Xu, J. Facile fabrication of robust superhydrophobic porous materials and their application in oil/water separation. *J. Mater. Chem. A* **2015**, *3* (46), 23252–23260.
- (19) Wu, Y.; Jia, S.; Qing, Y.; Luo, S.; Liu, M. A versatile and efficient method to fabricate durable superhydrophobic surfaces on wood, lignocellulosic fiber, glass, and metal substrates. *J. Mater. Chem. A* **2016**, *4* (37), 14111–14121.
- (20) Zhang, H.; Li, Y.; Lu, Z.; Chen, L.; Huang, L.; Fan, M. A robust superhydrophobic TiO₂ NPs coated cellulose sponge for highly efficient oil-water separation. *Sci. Rep.* **2017**, *7* (1), 9428.
- (21) Jiang, L.; Tang, Z.; Clinton, R. M.; Breedveld, V.; Hess, D. W. Two-Step Process To Create “Roll-Off” Superamphiphobic Paper Surfaces. *ACS Appl. Mater. Interfaces* **2017**, *9* (10), 9195–9203.

(22) Liu, S.; Zhou, H.; Wang, H.; Zhao, Y.; Shao, H.; Xu, Z.; Feng, Z.; Liu, D.; Lin, T. Argon Plasma Treatment of Fluorine-Free Silane Coatings: A Facile, Environment-Friendly Method to Prepare Durable, Superhydrophobic Fabrics. *Adv. Mater. Interfaces* **2017**, *4* (11), 1700027.

(23) Jiang, L.; Tang, Z.; Clinton, R. M.; Hess, D. W.; Breedveld, V. Fabrication of highly amphiphobic paper using pulp debonder. *Cellulose* **2016**, *23* (6), 3885–3899.

(24) Xie, L.; Tang, Z.; Jiang, L.; Breedveld, V.; Hess, D. W. Creation of superhydrophobic wood surfaces by plasma etching and thin-film deposition. *Surf. Coat. Technol.* **2015**, *281*, 125–132.

(25) Qing, Y.; Yang, C.; Hu, C.; Zheng, Y.; Liu, C. A facile method to prepare superhydrophobic fluorinated polysiloxane/ZnO nanocomposite coatings with corrosion resistance. *Appl. Surf. Sci.* **2015**, *326*, 48–54.

(26) Yang, M.; Liu, W.; Jiang, C.; He, S.; Xie, Y.; Wang, Z. Fabrication of superhydrophobic cotton fabric with fluorinated TiO₂ sol by a green and one-step sol-gel process. *Carbohydr. Polym.* **2018**, *197*, 75–82.

(27) Khanjani, P.; King, A. W. T.; Partl, G. J.; Johansson, L.-S.; Kostianinen, M. A.; Ras, R. H. A. Superhydrophobic Paper from Nanostructured Fluorinated Cellulose Esters. *ACS Appl. Mater. Interfaces* **2018**, *10* (13), 11280–11288.

(28) Zhao, H.; Park, K. C.; Law, K. Y. Effect of surface texturing on superoleophobicity, contact angle hysteresis, and “robustness”. *Langmuir* **2012**, *28* (42), 14925–34.

(29) Fan, M.; Dai, D.; Huang, B. Fourier transform infrared spectroscopy for natural fibres In *Fourier Transform-Materials Analysis*; InTech: 2012.

(30) Hundhausen, U.; Militz, H.; Mai, C. Use of alkyl ketene dimer (AKD) for surface modification of particleboard chips. *European Journal of Wood and Wood Products.* **2009**, *67* (1), 37–45.

(31) Yang, Q.; Saito, T.; Isogai, A. Facile fabrication of transparent cellulose films with high water repellency and gas barrier properties. *Cellulose* **2012**, *19* (6), 1913–1921.

(32) Wang, P.; Chen, M.; Han, H.; Fan, X.; Liu, Q.; Wang, J. Transparent and abrasion-resistant superhydrophobic coating with robust self-cleaning function in either air or oil. *J. Mater. Chem. A* **2016**, *4* (20), 7869–7874.

(33) Zhang, Z.-h.; Wang, H.-j.; Liang, Y.-h.; Li, X.-j.; Ren, L.-q.; Cui, Z.-q.; Luo, C. One-step fabrication of robust superhydrophobic and superoleophilic surfaces with self-cleaning and oil/water separation function. *Sci. Rep.* **2018**, *8* (1), 3869.